

MD Simulation of Structural and Mechanical Transformation of Single-Walled Carbon Nanotubes Under Pressure

Ji Zang¹, Oswaldo Aldás-Palacios^{1,2} and Feng Liu^{1,*}

¹ *Department of Materials Science and Engineering, University of Utah, Salt Lake City, UT 84112, USA.*

² *Visiting Professor, on sabbatical leave from the Escuela Politécnica Nacional, Quito-ECUADOR.*

Received 7 July 2006; Accepted (in revised version) 17 August 2006

Communicated by Leihan Tang

Available online 5 October 2006

Abstract. We investigate the structural and mechanical properties of single-walled carbon nanotubes (SWNTs) under hydrostatic pressure, using constant-pressure molecular dynamics (MD) simulations. We observed that all the SWNTs, independent of their size and chirality, behave like a classical elastic ring exhibiting a buckling transition transforming their cross-sectional shape from a circle to an ellipse. The simulated critical transition pressure agrees well with the prediction from continuum mechanics theory, even for the smallest SWNT with a radius of 0.4nm. Accompanying the buckling shape transition, there is a mechanical hardness transition, upon which the radial moduli of the SWNTs decrease by two orders of magnitude. Further increase of pressure will eventually lead to a second transition from an elliptical to a peanut shape. The ratio of the second shape transition pressure over the first one is found to be very close to a constant of ~ 1.2 , independent of the tube size and chirality.

PACS (2006): 81.07.De, 73.63.Fg, 85.35.Kt

Key words: Carbon nanotube, high-pressure solid-state phase transformation, MD simulation.

1 Introduction

The discovery of carbon nanotubes [1] has opened up a new area for experimental and theoretical research. Carbon nanotubes have exhibited many fascinating properties as well as intriguing structure-property relationships. For example, the mechanical properties of carbon nanotubes have been extensively studied, with a wide range of potential

*Corresponding author. *Email addresses:* zang@eng.utah.edu (J. Zang), oaldas@yahoo.com (O. Aldás-Palacios), fliu@eng.utah.edu (F. Liu)

applications, such as to be used as the strengthening elements in composites. Single-walled carbon nanotubes (SWNT) can be either metallic or semi-conducting depending on their size and chirality [2], and the correlations between their electrical property and mechanical deformation have been studied both experimentally [3–7] and theoretically [8–15] for potential applications as nano-elements in electromechanical devices [13, 16]. First-principles calculations have shown that armchair metallic SWNTs may become semiconductor under a large flattening distortion [15]; while band gap of zigzag semiconductor SWNTs display a high sensitivity to external strain [9].

One way to study the structural and mechanical properties of carbon nanotubes is by applying hydrostatic pressure. A number of high-pressure experiments have been carried out on bundles of SWNTs [17–21], showing pressure induced structural transitions in the range of 1-2 *GPa* [17–19]. Recent experiments also showed that pressure may induce transitions in electrical and magneto transport properties in SWNT bundles [22], which correlate closely with the pressure induced structural shape transitions [22]. In parallel, extensive theoretical studies, ranging from first-principles calculations [23–25], molecular dynamics (MD) simulations [25–27], to continuum mechanics modeling [25, 27] have been performed by several groups to study properties of both isolated single SWNTs and bundles of SWNTs under pressure.

For isolated single tubes, so far theoretical studies have mostly focused on armchair and zigzag tubes [25, 27] under pressure, which have a high symmetrical radial atomic structure and a short axial period. It has been shown that pressure induces a series of shape transitions in both armchair and zigzag SWNTs, transforming their cross sections from a circle to an elliptical and then from an elliptical to a peanut shape [27]. And a universal geometric constant was discovered to define these two shape transitions [27]. Furthermore, a mechanical (hardness) transition was found at the first shape transition, at which the radial moduli of SWNTs decrease by as much as two orders of magnitude [25]. Here, we report constant-pressure MD simulations of isolated SWNTs to investigate their shape and mechanical transitions under hydrostatic pressure. In particular, we extend previous works to chiral tubes to complete a systematic study of all three types of tubes (armchair, zigzag and chiral). We will present some details of the method for atomic volume partition in all three types of tubes, to facilitate the constant-pressure MD simulations of a finite system. Our simulations show that all three types of tubes behave, essentially, in the same manner under pressure. They follow closely the prediction of isotropic continuum mechanics analysis, down to the smallest tubes we simulated with a radius of 0.4nm.

2 Calculation details

The molecular dynamics (MD) method is a powerful simulation tool, widely used in chemistry, physics and materials science [28], but the traditional constant-pressure MD method is designed for an infinite system with periodic boundary conditions and cannot

be directly applied to a finite system in which there is no periodic boundary condition. Sun and Gong developed a constant-pressure MD simulation scheme for treating finite systems, in which the total volume of the system is partitioned into individual atomic volume that can be in turn expressed as a function of the atomic coordinates [29]. This method has been successfully used for simulations of Ni nanoparticles and carbon nanotubes [29], which we will adopt here. Briefly, one defines the Lagrangian L of an N -atom system as

$$L = \sum_i^N \frac{p_i^2}{2m_i} - (\phi\{r_i\} + P_{ext}V) \quad (2.1)$$

where r_i , m_i and p_i are the coordinate, mass and momentum of the i th atom, respectively. ϕ is the potential, V the volume and P_{ext} the external pressure. The key is to add the $P_{ext}V$ term into total energy. For a finite system, whose volume is not uniquely defined, we partition it as a summation of the volumes of individual atoms, V_i , as $V = \sum_i^N V_i$. V_i can be generally calculated by the method Voronoi polygon [30]. To treat a carbon nanotube, however, we have partitioned the atomic volume of different types of SWNTs as described below.

It is usually difficult to calculate the volume of an atom in an arbitrary cage structure because it can be ambiguous to assign the open volume in the cage to individual atoms. However, due to the high symmetry and the short period along the axial direction of the armchair and zigzag SWNTs, an effective way can be found for their atomic volume partition, as shown in Fig. 1a and 1b, respectively. The atomic volume of atom i (V_i) was partitioned by dividing the cross section of the nanotube into triangles multiplied by the single atomic-layer height, which was determined by the positions of atom i and its three nearest neighbors (j_1 , j_2 and j_3). Accordingly, the atomic volume can be expressed in terms of the atomic coordinates of these four atoms, i.e., $V_i = V_i(R_i, R_{j_1}, R_{j_2}, R_{j_3})$, as the following:

Armchair:

$$V_i = \frac{1}{2} \times [(Z_{j_2} - Z_{j_3}) \times S_{\Delta o'ij'_1} + (Z_{j_2} - Z_i) \times S_{\Delta o'ij'_2} + (Z_i - Z_{j_3}) \times S_{\Delta o'ij'_3}], \quad (2.2)$$

Zigzag:

$$V_i = \frac{1}{2} \times (Z_{j_3} - Z_{j_1}) \times (S_{\Delta o'ij'_1} + S_{\Delta o'ij'_2}), \quad (2.3)$$

with

$$S_{\Delta o'ij'_m} = \frac{1}{4} \sqrt{(r_i + r_{j_m} + d_{ij_m})(r_i + r_{j_m} - d_{ij_m})(r_i - r_{j_m} + d_{ij_m})(-r_i + r_{j_m} + d_{ij_m})}, \quad (2.4)$$

$$r_n = \sqrt{X_n^2 + Y_n^2}, \quad n = i, j_1, j_2, j_3, \quad (2.5)$$

$$d_{ij_m} = \sqrt{(X_i - X_{j_m})^2 + (Y_i - Y_{j_m})^2}, \quad m = 1, 2, 3. \quad (2.6)$$

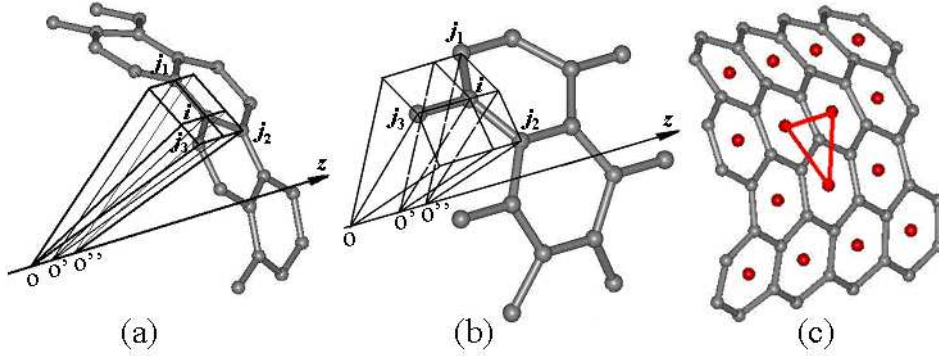


Figure 1: Atomic volume partition of (a) an armchair tube and (b) a zigzag tube. (c) Atomic surface area partition of a chiral tube.

Here, $S_{\Delta o'ij'_m}$ is the projection of $S_{\Delta o'ij_m}$ to the $Z_{o'}$ plane. The pressure-induced force on atom i is then calculated by taking the minus derivative of PV_i with respect to the coordinates of atom i .

For chiral SWNTs, the above partition for armchair and zigzag SWNTs is not applicable because of loss of symmetry. Instead, we used a different scheme by partitioning the atomic surface area, to avoid the issue for partitioning the open space in the tube to individual atoms, so as to account for the force applied by hydrostatic pressure to every atom. The force was calculated by the $P_{ext}S_i$ term, where S_i is the atomic area of a given atom, which is calculated as shown in Fig. 1c. The solid red dots are the center of mass of every hexagonal rings, so every carbon atom is surrounded by three solid red dots. We take the area of the triangle made of three solid red dots as the atomic area of the atom at the center. The direction of force is simply taken as the inverse normal direction of the triangular plane. This method is found to be rather effective, especially for large chiral tubes when the three dots surrounding an atom are almost in the same plane, as we compare our results of chiral tubes to those of armchair and zigzag tubes shown below.

We used Tersoff's many-body carbon potentials [31], which have been shown to work well for calculating the structural and mechanical properties of carbon nanotubes [32]. Periodic boundary conditions were used in the axial direction (z -direction) along the tube with one single unit cell and free boundary conditions in the radial direction. So effectively an infinite long isolated uncapped SWNT was simulated. Considering that nanotubes are orders of magnitude stiffer in the axial than in the radial direction, the relaxation in the z -direction was negligible in the studied pressure ranges, so the relaxation along the tube axis is neglected in the simulation.

MD simulations were carried out at the constant temperature of 300K and selected pressures, using the constant NPT Hoover Dynamics [33] with the fifth order predictor-corrector integration algorithm and a time step of 0.4fs. All the MD simulations ran for two million steps and the ensemble average for all the quantities were averaged over the last 500,000 steps. We also did static relaxation to obtain equilibrium structures using

R. M. Wentzcovitch's algorithm [34] with a time step of 0.85fs. The convergence criteria were set at $5 \times 10^{-5} eV/\text{\AA}$ for forces on all atoms. The equilibrium and MD structures were simulated for a wide range of SWNT sizes: from (6,6) to (20,20) for armchair tubes, from (10,0) to (35,0) for zigzag tubes, and from (12,3) to (20,10) for chiral tubes with their radii varying from 0.4nm to 1.4nm.

3 Results and discussion

3.1 Structural shape transitions

Fig. 2 shows the typical MD simulated cross sections of a (10,10) armchair SWNT at 300K as a function of pressure (P), demonstrating a series of shape transitions induced by pressure. Five snap shots with a time interval of 20 ps are shown at each pressure after equilibration. At $P=0$ (Fig. 2a), the tube maintains a circular "equilibrium" shape. Although a single snapshot of the cross section at any given time instance is not exactly a circle, the average of all the snap shots (cross sections) over a period of time is always a circle. This just indicates that the tube thermally fluctuates around its equilibrium circular shape.

At $P = 1.55 \text{ GPa}$ (Fig. 2b), the tube cross section transforms into an elliptical shape, exhibiting its first buckling shape transition, i.e., a spontaneous symmetry breaking transition into a structure of lower symmetry. Again, at any given time instance, thermal fluctuation makes the shape slightly distorted, but time average over many snap shots converges into a perfect elliptical shape, representing the characteristic shape for the given pressure. One notices that the tube rotates from one snap shot to the next, which is actually an artifact of the MD simulation. Due to the finite tube size (length) used in the simulation, when random velocities were initially assigned to all the atoms according to the temperature, a spurious residual angular momentum was artificially introduced, causing the system to rotate. For sufficiently long tubes, this residual momentum should be averaged out to zero over all atomic velocities. The same is true for simulations at all other pressures (see Figs. 2c and 2d).

At $P = 1.75 \text{ GPa}$ (Fig. 2c), the tube undergoes its second shape transition: transforming from an elliptical shape of all positive curvature along its perimeter (i.e., the convex shape), as shown in Fig. 2b, into a peanut shape containing two segments of negative curvature (i.e., nonconvex shape), as shown in Fig. 2d, with snap shots of cross sections at $P = 2.2 \text{ GPa}$. So, the second shape transition point is uniquely defined with a shape that contains two points of zero curvature, as shown in Fig. 2c, with a transition pressure of 1.75 GPa .

The same series of pressure induced structural shape transitions have been found in all three types of SWNTs we have simulated, which have also been shown by static structural relaxations at zero temperature. In general, the effect of finite temperature doesn't influence the general trend of pressure induced shape transitions, but only cause a thermal fluctuation around the equilibrium shape and a broadening of shape transitions, e.g., the transition pressure shown in Fig. 5. Thus, for the ease of comparison, we will use the

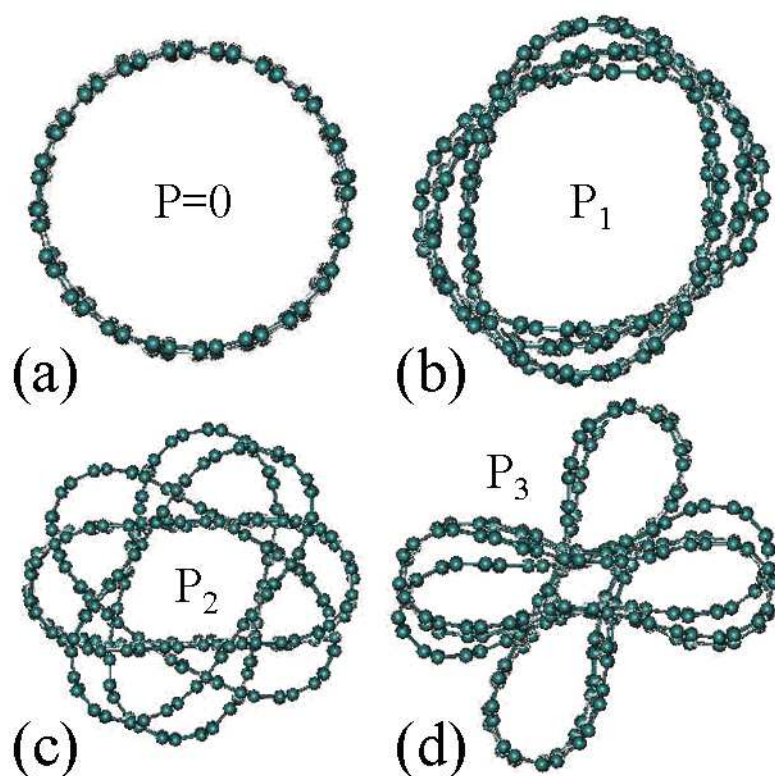


Figure 2: MD simulated cross sections of an armchair (10,10) SWNT at pressures of (a) 0, (b) 1.55, (c) 1.75, and (d) 2.2 GPa at 300K. There are 5 snapshots with a time interval of 20ps for every pressure.

equilibrium structures simulated at zero temperature to make a comparison with the continuum analysis, as discussed below.

As typical examples for illustration, Fig. 3 shows the tube cross sections of three different types of SWNTs under pressure obtained from static relaxation, including the (12,0) zigzag (Fig. 3a), the (12,6) chiral (Fig. 3b), and the (12,12) armchair (Fig. 3c) tubes. Independent of their chiralities and sizes, all three classes of tubes display the same series of shape transitions induced by pressure, with the red tube marking the first shape transition from circle to ellipse and the yellow tube marking the second transition from ellipse to peanut. The insensitivity on chirality indicates that the structural and mechanical properties of SWNTs are highly isotropic, with little directional dependence.

The first shape transition is a physical transition, which can be qualitatively well understood within the framework of continuum theory of buckling of elastic rings. For example, according to the continuum buckling theory [35–37], the transition pressure for the first shape transition from a circle to an ellipse occurs at a pressure of $P_1 = 3D/R_0^3$, where $D = Yt^3/12(1-\nu^2)$ is the tube flexural rigidity, Y is the Young's modulus, ν is the Poisson ratio, and t is the "effective" tube wall thickness; R_0 is the original tube radius.

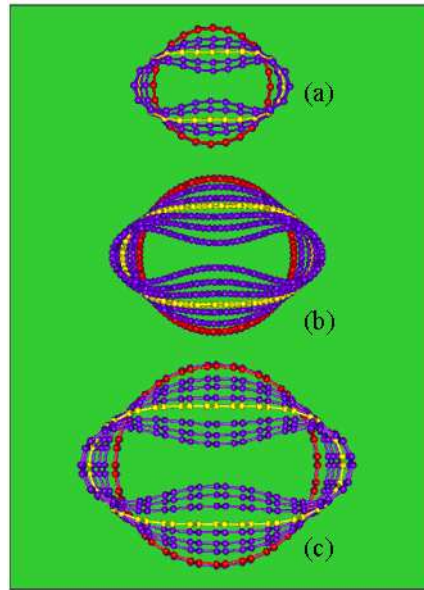


Figure 3: Evolution of cross-sections of SWNTs under hydrostatic pressure. (a) (12,0) zigzag, (b) (12,6) chiral, and (c) (12,12) armchair SWNT. The red tubes mark the first shape transition, and the yellow tubes mark the second shape transition, as discussed in the text.

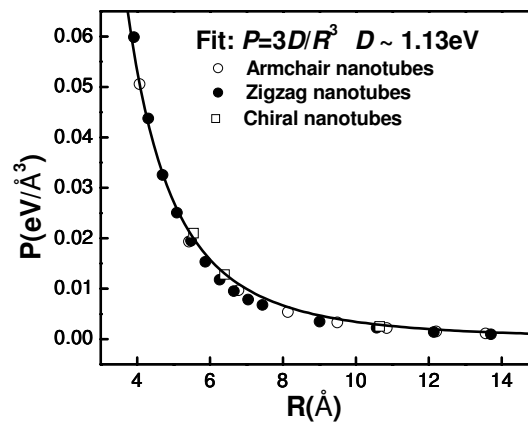


Figure 4: The dependence of the first transition pressures on tube radius and a fit to $P_1 = 3D/R^3$. Open circles: armchair tubes; Solid circles: zigzag tubes; Open squares: chiral tubes.

This relationship is indeed followed by all the SWNTs we have simulated, as shown in Fig. 4. By fitting the simulation results to this relation, we obtained the carbon nanotube flexural rigidity, $D \sim 1.13 \text{ eV}$, which differs by $\sim 30\%$ from the value of 0.85 eV obtained by Yakobson *et al.* [38] using a different interatomic potential and fitting to different tube deformations.

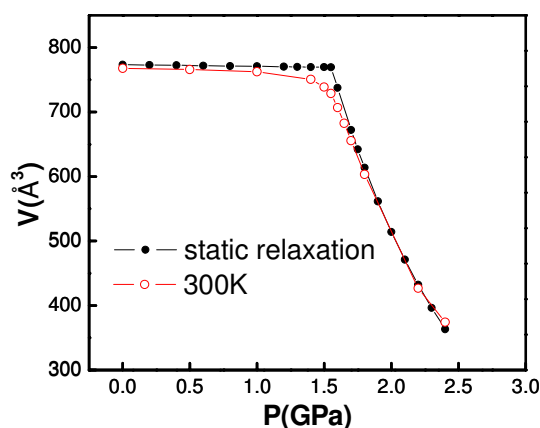


Figure 5: The volume of a (10,10) armchair SWNT as a function of pressure simulated at 0 and 300K.

3.2 Mechanical hardness transition

Accompanying the first circle-to-ellipse shape transition, the tubes exhibit also a mechanical transition, upon which the tube radial modulus may decrease by several orders of magnitude. This is clearly reflected in the plot of pressure-volume (P - V) relationships, as shown in Fig. 5 for the case of a (10,10) armchair SWNT as an example. One sees that there is drastic change in the slope of the P - V curve around the point of the first shape transition pressure of ~ 1.55 GPa. Below the transition pressure, the P - V curve has a rather small slope, indicating that the volume decreases only slightly with increasing pressure, characteristic of a “hard” phase. Above the transition pressure, the P - V has a much larger slope, indicating that the volume decreases rapidly with increasing pressure, characteristic of a “soft” phase. Also, the transition is very sharp at zero temperature (black dots and line), as obtained from static relaxation; while it is somewhat thermally broadened at the finite temperature of 300K (open circles and line), as obtained from MD simulations.

Such a correlated SWNT shape and hardness transition induced by pressure can be understood by continuum mechanics analysis [25, 27]. Imaging the hollow tube to be made of structureless membrane subject to outside hydrodynamic pressure that can be treated as a pressing force from outside, the tube will response to the increasing pressure (outside force) by adjusting its cross-section size and shape to generate an internal tensional force to balance the outside force. With increasing pressure, the circular tube initially shrinks its cross section from a radius R_0 to a smaller radius R . In doing so, the tube perimeter length is reduced from $(2\pi R_0)$ to $(2\pi R)$, which causes a compression strain energy of $E = C(1 - R/R_0)^2(\pi R)$, where $C = Yt/(1 - \nu^2)$ is the in-plane stiffness. In addition, the tube curvature along the perimeter is increased from $(1/R_0)$ to $(1/R)$, which causes an increase of bending strain energy of $E = \pi D(1/R - 1/R_0)$. Consequently, to maintain the circular shape, the tube must increase both its compression and bending strain energy with increasing pressure as its radius decreases. Because it usually costs

much higher energy to compress a beam than to bend a beam (Microscopically, this is to say that it is much harder to change bond length than to change bond angle [25]), at certain point the tube perimeter length becomes no longer compressible. But on the other hand, the tube cross sectional area must continue to decrease with increasing pressure, and then the only way to do so is for the tube to “buckle” into an elliptical shape with the same perimeter length but smaller area, since the circle has the largest area among all the possible shapes for the given perimeter length.

The above is the underlying physical reason driving the first shape transition, as was actually realized more than one century ago [35] in the terms of classical theory of buckling of elastic rings. One can view the tube cross section as a ring of atomic beads connected with elastic spring coils in between. As the ring shrinks under pressure, the spacing of coils continues to decrease until hitting a point that the coils are touching each other. At this point, the length of spring and hence the perimeter length of the ring can't decrease anymore, so the ring buckles into an elliptical shape to decrease its enclosed area under pressure. The buckling is a spontaneous process, which may occur at any point of “bead” along the ring randomly. But as long as it occurs it will continue along the same path.

On the same principle, one can easily understand the mechanical hardness transition associated with the buckling shape transition. Below the transition pressure, the circular tube shrinks with cost of both compression and bending strain energy, so it is relatively hard to shrink behaving as a hard phase. The radial modulus of this hard phase can be analytically derived by taking derivative of both these two energy terms with the respect to tube radius, as $B_h = C/2R_0 + 3D/4R_0^3 \approx C/2R_0$. So, the modulus of the hard phases is dominated by compression, which decreases approximately linearly with increasing radius; the larger the tube, the softer the tube. This relationship is indeed followed by all the simulation results, as shown in Fig. 6a. Here, the simulation data are obtained from the numerically derived slopes of P - V curves for the part below the transition pressure, as typically shown in Fig. 5. By fitting the data for all the tube types and sizes, we obtained the tube in-plane stiffness constant, $C = 26.12eV/\text{\AA}^2$.

Above the transition pressure, the tube changes into an elliptical shape of approximately constant perimeter length. It shrinks (reducing its cross-section area) with cost of only bending strain energy, so it is relatively easy to shrink behaving as a soft phase. The radial modulus of this soft phase can't be analytically derived, because the actual shape changing with pressure is not analytically expressible, as they fall into a family of different elliptical curves [27, 39]. For example, they start with shapes like an ellipse and change later into a peanut. Sun *et al.* had derived the modulus of the soft phase as $B_s = 19D/R_0^3$, using the simplest elliptical function $x^2/a^2 + y^2/b^2 = 1$ to represent the soft-phase shape [25]. But this turned out to be an overestimate of more than six times too big. Instead, we have derived numerically from our simulations that the modulus of the soft phase is $B_s = 3D/R_0^3$, as shown in Fig. 6b. This has also been confirmed by more elaborated variational geometric analysis using minimum-energy elastica [39]. It indicates that the simple elliptical shape assumed by Sun *et al.* is not of the lowest bend-

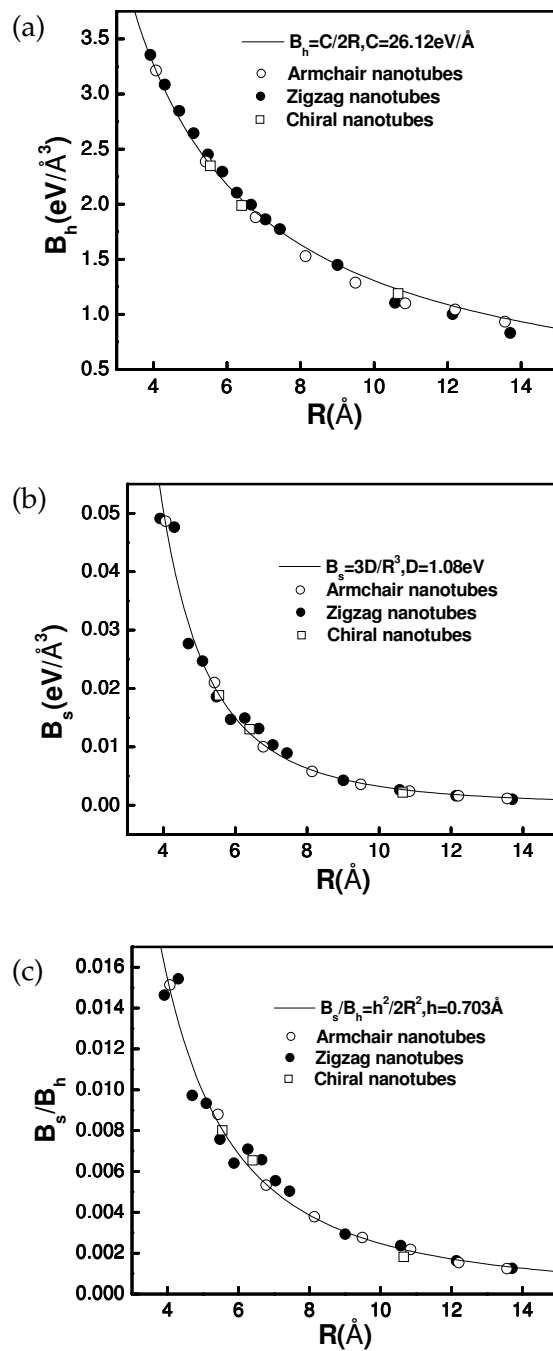


Figure 6: The bulk modulus of (a) hard phase, (b) soft phase and (c) the ratio of bulk modulus in the soft to hard phase, as a function of SWNT radius. Dots are simulated data and lines are fittings to the derived analytical expressions.

ing energy among all the possible elliptical functions that the tube can take. By fitting to the expression of $B_s = 3D/R_0^3$ with the data simulated from all the tube types and sizes shown in Fig. 6b, we obtained the tube flexural rigidity, $D \sim 1.08eV$. This agrees excellently with the value of $1.13eV$ obtained above from fitting the simulation data of the first transition pressure. So, in turn, such an excellent agreement reconfirms the correctness of the expression of the soft-phase modulus used for the fitting, which happens to be the same as the expression of the transition pressure, $P_1 = 3D/R_0^3$. However, the physical link between the two is not clear, as the expression for the soft-phase modulus could not be derived analytically but only empirically by numerical fitting.

Given the expressions of the tube radial modulus in the two phases below and above the first shape transition, it is straightforward to show that the ratio of the modulus of the soft phase over the hard phases is $B_s/B_h = t^2/2R_0^2$, which scales quadratically with the ratio of the “effective” tube wall thickness (t) over the tube radius (R_0). In general, t is about one to two orders magnitude smaller than R_0 , so B_s is typically several orders of magnitude smaller than B_h . This is quantitatively shown in Fig. 6c, where we plot the simulated data of B_s/B_h , falling in the range of $\sim 10^{-2}$ to 10^{-3} , as a function of R_0 . Also, all the data independent of tube type and size follow closely the expected relationship of $B_s/B_h = t^2/2R_0^2$. By fitting the data to this relationship, we obtained the tube effective wall thickness to be $t \sim 0.7\text{\AA}$, which agrees well with the previously estimated values of 0.66\AA [38].

3.3 Scaling relation between the two shape transitions

Another very interesting discovery on the pressure induced SWNT shape transitions is there exists a universal constant relating the second shape transition to the first one [27]. This was first realized from simulations as shown in Fig. 7, where the ratio of the tube cross-sectional areas at the second transition (A_2) over those at the first transition (A_1) is plotted as a function of tube radius for all three types of SWNTs studied. Apparently, this ratio appears to be a constant of ~ 0.82 , independent of tube size and chirality. This indicated the existence of a geometric constant, because the second transition is a purely geometric transition, which does not give rise to changes in the tube’s physical properties. For example, mechanically, the first transition changes the tube’s behavior under pressure from both compression and bending to pure bending, while the second transition changes only the tube geometry from a convex to nonconvex shape. Beyond the first shape transition, the tube continues to deform by pure bending passing through the second shape transition point.

The existence of such a universal geometric constant was then proved by formulating a variational geometrical problem to minimize bending energy of a family of closed plane curves with fixed arc length [27,39]. The solutions (minimum-energy curves of elastica) of this variational problem represent correctly the cross-sectional shape evolution of SWNTs under pressure, as illustrated in Fig. 8, in which we compare the mathematical solutions of curves (black lines) with the simulated atomic positional contours, and the two match

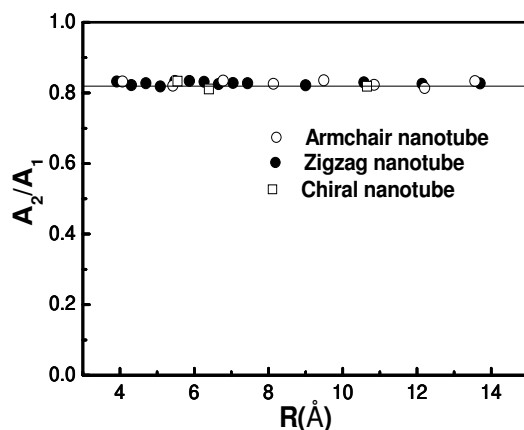


Figure 7: The ratio of the simulated tube cross-section areas at the second shape transition point (yellow tube in Fig. 3) to those at the first transition (red tube in Fig. 3). The ratio appears to be constant ~ 0.82 , as indicated by the straight line. The small data variations are due to uncertainties in determining the exact shape transition points.

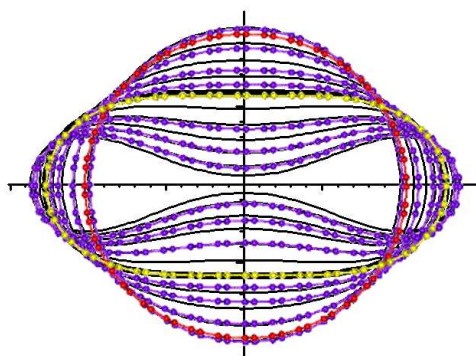


Figure 8: Evolution of cross-sections of SWNTs under hydrostatic pressure, illustrating the perfect agreement between the solutions of variational geometry analysis (black lines) and atomistic simulations of a (18,18) tube. The color dots are atoms with the red marks the first shape transition and the yellow the second.

each other perfectly. The variational analysis indeed confirmed the existence of such a geometric constant [27, 39]. Further, it facilitated the numerical computation of the accurate value of this geometric constant, an irrational number to be 0.819469.

The existence of this geometric constant relating the second and the first shape transition indicates also that there will be a scaling relation between the first and second transition pressure. Based on continuum elastic theory, the pressure and the cross-sectional area at the two transition points are related as $P_1 - P_2 = B_s \ln(A_2/A_1)$. Here B_s is the radial modulus of the SWNT in the soft phase between P_1 and P_2 . We have shown above that B_s and P_1 have the same expression, i.e., $B_s = P_1 = 3D/R_0^3$. Then, we obtain $P_2/P_1 = 1 - \ln(A_2/A_1) \approx 1.2$, as A_2/A_1 is the constant of ~ 0.82 . This is indeed confirmed by our simulations as shown in Fig. 9.

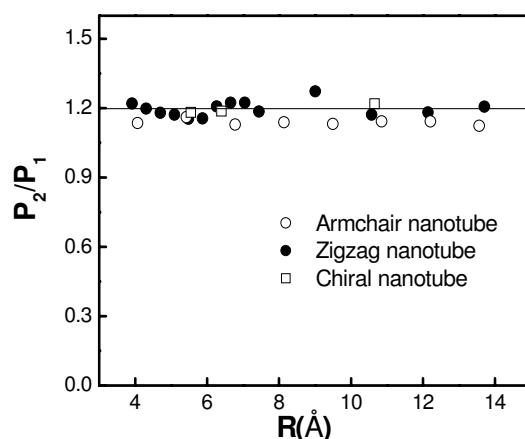


Figure 9: Simulated ratio of the second transition pressure (P_2) to the first (P_1) as a function of SWNT radius.

Such scaling relations of transition pressures can be useful in designing carbon nanotube pressure sensors [16]. It has been shown that if the pressure is increased further beyond the second shape transition to drive the tube into a peanut shape, eventually it will cause an electrical tube transition, making an armchair metal tube semiconducting due to additional tube wall interaction [16]. This provides a unique electromechanical mechanism for sensing pressure, for which scaling relationships are used for pressure calibration.

4 Summary

In summary, we have carried out extensive MD dynamics simulations of SWNTs, to investigate their structural and mechanical properties under hydrostatic pressure. We show a series of pressure induced tube cross-sectional shape transitions. First, the tube transforms from a circle to an ellipse, driven by a competition between the energy penalties of compressing vs. bending the tube. Second, the tube transforms from an ellipse to a peanut, as a pure geometric transformation from a convex to nonconvex shape without changing the tube physical properties (such as the harness). Accompanying the first circle-to-ellipse shape transition, the tube exhibits also a hard-to-soft mechanical transition, upon which the radial moduli of the SWNTs decrease by several orders of magnitude. Further, there exists a universal geometric constant and scaling relationship in pressure between the first and the second shape transition. All the pressure induced structural and mechanical transitions of SWNTs, as obtained from simulations, are shown to be well described by continuum mechanics theory even for the smallest tube studied with a radius of ~ 0.4 nm. These include qualitative scaling relations as well as quantitative elastic parameters, i.e., the critical pressure of the first transition, the radial moduli of the soft and hard phases and their ratio, and the geometric constant defining the sec-

ond to first shape transition, etc. The SWNTs are found to be highly isotropic in their structural and mechanical behavior, with all the properties studied to be independent of chirality.

Acknowledgments

This work is partly supported by DOE (DE-FG03- 01ER45875; -03ER46027). O. Aldás-Palacios is partly supported by NSF (DMR0307000).

References

- [1] S. Iijima, *Nature* 354 (1991) 56.
- [2] R. Saito, M. Fujita, G. Dresselhaus, M.S. Dresselhaus, *Appl. Phys. Lett.* 60 (1992) 2204.
- [3] T. W. Tombler, C. Zhou, L. Alexseyev, J. Kong, H. Dai, L. Liu, C.S. Jayanthi, M. Tang, S.Y. Wu, *Nature (London)* 405 (2000) 769.
- [4] J. Cao, Q. Wang, H. Dai, *Phys. Rev. Lett.* 90 (2003) 157601.
- [5] A. Bezryadin, A.R.M. Verschueren, S.J. Tans, C. Dekker, *Phys. Rev. Lett.* 80 (1998) 4036.
- [6] S. Paulson, M.R. Falvo, N. Snider, A. Helser, T. Hudson, A. Seeger, R.M. Taylor, R. Superfine, S. Washburn, *Appl. Phys. Lett.* 75 (1999) 2936.
- [7] T. Kuzumaki, Y. Mitsuda, *Appl. Phys. Lett.* 85 (2004) 1250.
- [8] P. E. Lammert, P. Zhang, V.H. Crespi, *Phys. Rev. Lett.* 84 (2000) 2453.
- [9] M.S.C. Mazzoni, H. Chacham, *Appl. Phys. Lett.* 76 (2000) 1561.
- [10] R. Heyd, A. Charlier, E. McRae, *Phys. Rev. B* 55 (1997) 6820.
- [11] A.A. Farajian, B.I. Yakobson, H. Mizuseki, Y. Kawazoe, *Phys. Rev. B* 67 (2003) 205423.
- [12] A. Maiti, A. Svizhenko, M.P. Anantram, *Phys. Rev. Lett.* 88 (2002) 126805.
- [13] O. Glseren, T. Yildirim, S. Ciraci, C. Kilic, *Phys. Rev. B* 65 (1997) 155410.
- [14] W. Guo, Y. Guo, *Phys. Rev. Lett.* 91 (2003) 115501.
- [15] J.Q. Lu, J. Wu, W. Duan, F. Liu, B.F. Zhu, B.L. Gu, *Phys. Rev. Lett.* 90 (2003) 156601.
- [16] J. Wu, J. Zang, B. Larade, H. Guo, X.G. Gong, F. Liu, *Phys. Rev. B* 69 (2004) 153406.
- [17] M.J. Peters, L.E. McNeil, J.P. Lu, D. Kahn, *Phys. Rev. B* 61 (2000) 5939.
- [18] J. Tang, L.C. Qin, T. Sasaki, M. Yudasaka, A. Matsushita, S. Iijima, *Phys. Rev. Lett.* 85 (2000) 1887.
- [19] U.D. Venkateswaran, A.M. Rao, E. Richter, M. Menon, A. Rinzler, R.E. Smalley, P.C. Eklund, *Phys. Rev. B* 59 (1999) 10928.
- [20] S. Rols, I.N. Goncharenko, R. Almairac, J.L. Sauvajol, I. Mirebeau, *Phys. Rev. B* 64 (2001) 153401.
- [21] S.M. Sharma, S. Karmakar, S.K. Sikka, P.V. Teredesai, A.K. Sood, A. Govindaraj, C.N.R. Rao, *Phys. Rev. B* 63 (2001) 205417.
- [22] J.Z. Cai, L. Lu, W.J. Kong, H.W. Zhu, C. Zhang, B.Q. Wei, D.H. Wu, F. Liu, *Phys. Rev. Lett.* 97 (2006) 026402.
- [23] M.H.F. Sluiter, V. Kumar, Y. Kawazoe, *Phys. Rev. B* 65 (2002) 161402.
- [24] S. P. Chan, W.L. Yim, X.G. Gong, Z.F. Liu, *Phys. Rev. B* 68 (2003) 075404.
- [25] D.Y. Sun, D.J. Shu, M. Ji, F. Liu, M. Wang, X.G. Gong, *Phys. Rev. B* 70 (2004) 165417.
- [26] X.H. Zhang, D.Y. Sun, Z.F. Liu, X.G. Gong, *Phys. Rev. B* 70 (2004) 035422.
- [27] J. Zang, A. Treibergs, Y. Han, F. Liu, *Phys. Rev. Lett.* 92 (2004) 105501.

- [28] M.P. Allen, D.J. Tildesley, *Computer Simulation of Liquids*, Clarendon Press, Oxford, 1977.
- [29] D.Y. Sun, X.G. Gong, *J. Phys.-Condens. Mat.* 14 (2002) L487.
- [30] F. Aurenhammer, *ACM Comput. Surv.* 23 (1991) 345.
- [31] J. Tersoff, *Phys. Rev. B* 39 (1989) 5566.
- [32] J. Tersoff, R. Ruoff, *Phys. Rev. Lett.* 73 (1994) 676.
- [33] S. Melchionna, G. Ciccotti, B.L. Holian, *Mol. Phys.* 78 (1993) 533.
- [34] R.M. Wentzcovitch, J.L. Martins, G.D. Price, *Phys. Rev. Lett.* 70 (1993) 3947.
- [35] M. Levy, *J. Math. Ser.* 3 (1884) 7.
- [36] G.F. Carrier, *J. Math. Phys.* 26 (1947) 94.
- [37] J. Chaskalovic, *Z. Angew. Math. Phys.* 46 (1995) 149, and references therein.
- [38] B.I. Yakobson, C.J. Brabec, J. Bernholc, *Phys. Rev. Lett.* 76 (1996) 2511.
- [39] A. Treibergs, F. Liu, to be published.